

# Non-Prehensile Object Transport by Nonholonomic Robots Connected by Linear Deformable Elements

Hui Zhi, Bin Zhang, Jiaming Qi, *Member, IEEE*, Jose Guadalupe Romero, *Member, IEEE*, Xiaodong Shao, Chenguang Yang, *Fellow, IEEE*, and David Navarro-Alarcon, *Senior Member, IEEE*

**Abstract**—This paper presents a new method to automatically transport objects with mobile robots via non-prehensile actions. Our proposed approach utilizes a pair of nonholonomic robots connected by a deformable tube to efficiently manipulate objects of irregular shapes toward target locations. To autonomously perform this task, we develop a local integrated planning and control strategy that solves the problem in two steps (*viz.* enveloping and transport) based on the model predictive control (MPC) framework. The deformable underactuated system is simplified by a linear kinematic model. The enveloping problem is formulated as the minimization of multiple criteria that represent the enclosing error of the object by the variable morphology system. The transport problem is tackled by formulating the non-prehensile dragging action as an inequality constraint specified by the body frame of the deformable system. Reactive obstacle avoidance is ensured by a maximum margin-based term that utilizes the system's geometry and the feedback proximity to the environment. To validate the performance of the proposed methodology, we report a detailed experimental study with vision-guided robotic prototypes conducting multiple autonomous object transport tasks.

**Index Terms**—Nonprehensile manipulation; Motion control; Object transport; Deformable agents; Nonholonomic systems.

## I. INTRODUCTION

Manipulation of rigid objects has a rich history in robotics, where many important results have been achieved in the last few years. Traditional approaches—relying on fixed-base robot arms with customized end-effectors—can only be used with objects that satisfy special conditions. For example, geometries suitable for grasping [1] or flat surfaces for suction lifting [2]. Mobile robots can perform manipulation tasks without the need to use end-effectors [3], e.g., they can transport objects by dragging them through deformable ropes or cables. This type of (non-prehensile) strategy is useful in alleviating some of the drawbacks of traditional approaches, as it enables to

Manuscript received: March 5, 2024; Revised: June 17, 2024; Accepted: July 24, 2024. This paper was recommended for publication by Editor Yong-Lae Park upon evaluation of the Associate Editor and Reviewers' comments. This work was supported by the Research Grants Council under grant number 15231023. *Corresponding author: David Navarro-Alarcon.*

Hui Zhi, Bin Zhang, and David Navarro-Alarcon are with the Department of Mechanical Engineering, The Hong Kong Polytechnic University (PolyU), KLN, Hong Kong. [hui1225.zhi@connect.polyu.hk](mailto:hui1225.zhi@connect.polyu.hk), [bin.zhang@connect.polyu.hk](mailto:bin.zhang@connect.polyu.hk), [dna@ieee.org](mailto:dna@ieee.org)

Jiaming Qi is with the Centre for Transformative Garment Production of the University of Hong Kong, NT, Hong Kong. [jiaming.qi@ieee.org](mailto:jiaming.qi@ieee.org)

Jose Guadalupe Romero is with the Instituto Tecnológico Autónomo de México, Mexico City, Mexico. [jose.romerovelazquez@itam.mx](mailto:jose.romerovelazquez@itam.mx)

Xiaodong Shao is with the School of Automation Science and Electrical Eng., Beihang University, Beijing, China. [xdshao\\_sasee@buaa.edu.cn](mailto:xdshao_sasee@buaa.edu.cn)

Chenguang Yang is with Department of Computer Science, University of Liverpool, Liverpool, United Kingdom. [cyang@ieee.org](mailto:cyang@ieee.org)

Digital Object Identifier (DOI):

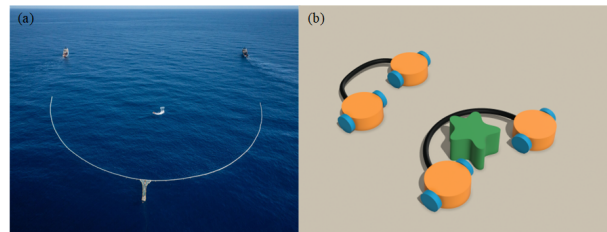


Fig. 1. (a) Ocean Cleanup system using two deformable wings to collect debris. (b) Conceptual model of our proposed approach to envelop and transport an irregular object.

manipulate objects with un-graspable geometries, increases the operation range of the transportation task, and combines the power of multiple robots to move larger loads, among others. Consequently, these types of strategies are potentially useful in many important applications, such as clearing debris from water [4] (Fig. 1. (a)), transporting materials in construction sites [5], or even in domestic cleaning tasks [6]. Despite its evident practical value, the development of non-prehensile controls that exploit deformable materials to indirectly manipulate objects is still an understudied problem in the robotics community.

Many researchers have studied the automatic transportation of objects by mobile agents considering several types of configurations (see [7] for a comprehensive literature review). For agents equipped with arms or grippers, the task can be collaboratively performed by the robot fleet through formation control strategies [8]. This approach was used in [9], [10], where motion planning algorithms were developed to manipulate both rigid and deformable objects with multi-robot systems. These strategies have also been formulated using constrained optimization subject to kinematic/dynamic constraints. For simple agents that lack active grippers, a common method to transport the load is to physically enclose it with the robots' structure while maintaining a fixed formation throughout the path to ensure a stable mobile grasp [11].

In contrast to gripper-based approaches, the use of dragging/pushing enables the transport of objects with fewer and mechanically simpler robots. A key challenge with these strategies is the presence of uncertain frictional forces [12], which complicate the object's positioning. Several works have tried to address this issue. For example, [13] proposes a model predictive control (MPC) for nonholonomic robots taking into consideration the constraints associated with the pushing direction, [14] describes an algorithm to compute the optimal contact points to ensure the object's maneuverability along

the path, [15] presents a complete behavioral, reactive, and centralized framework for a multi-agent system to push a set of objects, [16] addresses the transport of non-rigid loads by using differentiable soft-body physics engines, to name a few instances. These previous works have established a solid foundation for the non-prehensile manipulation problem. Besides, the application of the passive structure, especially deformable materials, has shown potential in object transport. [17] developed a cooperative path-planning framework for a robot duo tethered by a flexible net to gather scattered objects. [18] also proposed a ball-string-ball structure used for transporting small objects. However, more research is still needed to develop non-prehensile models/controls for mobile agents composed of deformable elements. The aim of this paper is to provide a solution to this open problem.

To perform the task, our proposed system is composed of two nonholonomic mobile bases linked by a flexible tube that provides a large contact area (or multiple interaction points) with the object. This feature enhances the system's manipulation capabilities, yet its non-rigid nature complicates the development of planning and control algorithms. Note that most existing methods are designed for rigid systems with a fixed morphology [19]. To deal with this non-rigid nature, this paper proposes a new integrated planning and control strategy based on the MPC framework for deformable mobile agent systems, which provides efficient local motion control while incorporating obstacle avoidance and object manipulation capabilities. The proposed solution is divided into two stages: *enveloping*, where the object is enclosed by the tube, and *transport*, where the object is pulled towards a receptacle. The original contributions of this work are outlined as follows:

- 1) We formulate a constrained optimization problem of the enveloping task based on a gradient update rule that balances two optimization targets: the position and orientation of the flexible mobile system.
- 2) We derive an inequality constraint for the non-prehensile actions of the overall transportation system (combining the manipulated object and the flexible agent) that efficiently provides the pulling directions to reach the goal.
- 3) We design a new maximum-margin-based obstacle avoidance method for this deformable robot that prevents "hugging" an obstacle.

A series of real-world experiments are conducted to evaluate the performance of this new methodology in handling a diverse range of objects and obstacles.

## II. PRELIMINARIES AND PROBLEM STATEMENT

### A. Flexible Mobile System

The proposed system has two parts: active control components (two nonholonomic mobile robots) and passive deformation components (a deformable tube). The motion state of the end robot  $i$  is represented by  $\mathbf{p}_i = [x_i, y_i, \theta_i]^T \in \mathbb{R}^3$ ,  $i = 1, 2$ , of which the kinematic is

$$\dot{\mathbf{p}}_i = \begin{bmatrix} \dot{x}_i \\ \dot{y}_i \\ \dot{\theta}_i \end{bmatrix} = \begin{bmatrix} \cos \theta_i & 0 \\ \sin \theta_i & 0 \\ 0 & 1 \end{bmatrix} \begin{bmatrix} v_i \\ \omega_i \end{bmatrix} = \mathbf{R}(\theta_i) \mathbf{u}_i \quad (1)$$

where  $(x_i, y_i)$  is the position and  $\theta_i$  is the orientation of the robot  $i$ . And  $v_i$  and  $\omega_i$  are the linear and angular velocities of each robot, respectively. The input control is represented as  $\mathbf{u}_i = [v_i, \omega_i]^T$ .

The connected tube is a type of pneumatic tubing manufactured using polyurethane (PU) material, featuring an outer diameter of 6 mm and an inner diameter of 4 mm. The elasticity of the tube allows it to be easily bent by the two end robots. In our task, the longitudinal stretching of the tube is negligible and only the bending in our 2D platform is considered. The ring components are used to connect the tube end and the end mobile robots. This passive joint is not rigidly attached to the robot so that the tube end can rotate freely. Then, the shape of the tube is not affected by the orientation of the robots  $\theta_i$ . Thus, the configuration of the tube depends only on the controllable positions of the two mobile robots, which makes the effect of nonholonomic properties of mobile robots negligible.

### B. Enveloping Problem Statement

The first challenge addressed here is to model the kinematics of the proposed flexible mobile system and control it to envelop the target object without collision. To simplify the representation of the deformable tube,  $m$  points are evenly selected as the feature points of the tube, of which the state is represented by  $\mathbf{q}_j = [x_j^f(t), y_j^f(t)]^T \in \mathbb{R}^2$ ,  $j = 1, \dots, m$ . It is noticed that to get the middle point of the tube directly, the number  $m$  must be odd. We model the curved geometry of the deformable tube as an unknown nonlinear function  $\mathbf{q} = \mathbf{f}(\boldsymbol{\psi})$ , where  $\mathbf{q} = [\mathbf{q}_1^T, \mathbf{q}_2^T, \dots, \mathbf{q}_m^T]^T \in \mathbb{R}^{2m}$  denotes the position of the feature points, and  $\boldsymbol{\psi} = [x_1, y_1, x_2, y_2]^T \in \mathbb{R}^4$  represents the feedback position of the mobile bases. With this function, we obtain the following shape-motion model of the system:

$$\dot{\mathbf{q}} = \frac{\partial \mathbf{f}}{\partial \boldsymbol{\psi}} \dot{\boldsymbol{\psi}} = \mathbf{J}(\boldsymbol{\psi}) \dot{\boldsymbol{\psi}} \quad (2)$$

for  $\mathbf{J}(\boldsymbol{\psi}) \in \mathbb{R}^{2m \times 4}$  as the Jacobian matrix, whose analytical computation requires knowledge of the physical parameters of the tube, which are hard to obtain in practice. This structure can be numerically estimated from feedback data [20]. In this paper, the Least Square Method is used to fit the dynamic model (2) and to estimate the Jacobian matrix  $\mathbf{J}(\boldsymbol{\psi})$ , based on the sampled data of position changes of the feature points and end robots during the sample time  $\Delta t$ :  $\Delta \mathbf{q} = \mathbf{q}(t + \Delta t) - \mathbf{q}(t)$  and  $\Delta \boldsymbol{\psi} = \boldsymbol{\psi}(t + \Delta t) - \boldsymbol{\psi}(t)$ .

Different from the existing research, the proposed system has little requirement for the shape of the objects due to the application of the deformable tube. The contact point or surface of contact between the tube and the target object is not predetermined strictly, which holds greater significance when dealing with objects of irregular shapes. Thus, as shown in the left subfigure of Fig. 2, the target object can be represented by its minimum enclosing circle in 2-D. The position of the target object is defined as the center point  $\mathbf{p}_t$  of the minimum enclosing circle with the radius  $r_t$ .

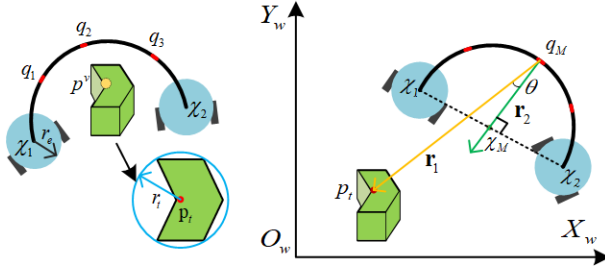


Fig. 2. (left) Illustration of the envelope completion status and the minimum enclosing circle of the irregular object. (right) The relative orientation between the target object and our system during the enveloping progress

To explain the enveloping task, the virtual geometric center point  $\mathbf{p}^v$  of the proposed system (shown in the left subfigure of Fig. 2)) is given, which is defined as

$$\mathbf{p}^v = \frac{1}{m+2} \left( \sum_{i=1}^2 \chi_i + \sum_{j=1}^m \mathbf{q}_j \right) \quad (3)$$

where  $\chi_i = [x_i, y_i]^T$  is the position of the mobile robot. We note that the proposed system can only handle the target object within a certain size that can be represented by:

$$r_t < \min(\|\mathbf{q}_j - \mathbf{p}^v\|, \|\chi_i - \mathbf{p}^v\| - r_e) \quad (4)$$

where  $r_e$  is the radius of the end mobile robot. Besides, considering that this system can only envelop the target from its “open” side that has no tube connected, the relative orientation of the system to the target object is considered and regarded as another target of the optimization. As shown in the right subfigure of Fig. 2, the direction of the system (the green arrow) is defined as the vector from the middle feature points  $\mathbf{q}_M$  of the tube to the virtual middle point  $\chi_M$  of the two end robots, while the yellow arrow shows the relative direction between the object and the flexible mobile agent system. Then, the relative orientation  $\theta$  is defined as the angle between these two vectors, which can not be obtained by the camera directly and is calculated by

$$\theta = \arccos \left( \frac{\mathbf{r}_1 \cdot \mathbf{r}_2}{\|\mathbf{r}_1\| \|\mathbf{r}_2\|} \right) \quad (5)$$

where  $\mathbf{r}_1 = \mathbf{p}_t - \mathbf{q}_M$ ,  $\mathbf{r}_2 = \chi_M - \mathbf{q}_M$ , with  $\chi_M = (\chi_1 + \chi_2)/2$  and  $\mathbf{q}_M = \mathbf{q}_{(m+1)/2}$ . Then, the enveloping task can be defined as follows.

**Problem 1.** Develop an MPC-based control method for the flexible mobile agent system (1)–(2), to automatically envelop an irregular-shaped object (i.e.,  $\mathbf{p}^v \rightarrow \mathbf{p}_t$  and  $\theta \rightarrow 0$ ) whose dimension satisfies (4), and to reactively avoid any collisions with the object, obstacles, and the bounded environment.

### C. Transport Problem Statement

As for the transport process, the challenge is to control the motion of the transported object pulled by the tube to the target receptacle. The transported object and the flexible mobile agent system are regarded as one new transport system. We assume that inertial forces are negligible or quickly absorbed by the frictional effects, i.e., quasi-static assumption. Due to

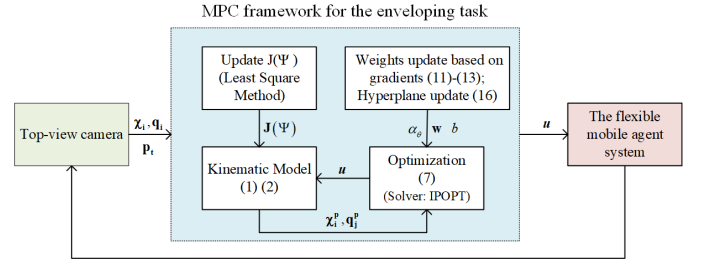


Fig. 3. Schematic overview of the framework for the enveloping task

the slip between the tube and the transported object and the complex physical properties of the tube, the whole transport system has a highly unstable and nonlinear dynamic. For this new system, the position of the object  $\mathbf{p}_t$  is regarded as part of the state instead of the shape of the tube. Similarly, we define the kinematics model of the transported object as

$$\dot{\mathbf{p}}_t = \mathbf{J}_t(\psi) \dot{\psi} \quad (6)$$

where  $\mathbf{J}_t(\psi) \in \mathbb{R}^{2 \times 4}$  represents how end mobile robots change the motion of the transported object during transport. The matrix  $\mathbf{J}_t(\psi)$  must be updated in real-time because the object is not fixed to the tube and may slide along it. We still use the update algorithm in [20] to update the matrix  $\mathbf{J}_t(\psi)$  using the visual feedback information.

The target receptacle is given as a rectangle zone  $R_z$ , of which the geometry center is represented by  $T_z \in \mathbb{R}^2$ . Then, the transport problem can be given as:

**Problem 2.** Develop an MPC-based local control method for the whole transport system described by (1) and (6), to automatically deliver the transported object into the receptacle (i.e.,  $\mathbf{p}_t \in R_z$ ), while avoiding collisions.

## III. METHODOLOGY

In our framework, the optimization problems of envelopment and transport tasks are formulated, and the real-time update methods of the MPC algorithm are given.

### A. Enveloping Problem Formulation

To control the flexible deformable mobile agent system to envelop the target object without any collision with the obstacle and the target object in the bounded environment, we present a novel MPC formulation to calculate the control input  $u_i$  of the two end robots, as shown in Fig. 3. The finite forecast horizon is set as  $n$  steps with the sampling time  $T_s$ . This MPC is constrained by (i) dynamics (1)–(2), (ii) bounds on control input, (iii) position bounds, (iv) distance range between the two end robots, (v) collision avoidance with the target object, and (vi) obstacle avoidance with the environment. And (v) and (vi) are designed as soft constraints in the objective function. The optimal tasks contain the control input, the distance error and the relative orientation. Then, for the predicted state estimate

at each discrete-time instant  $k$ , this multi-task constrained optimization problem is formulated as

$$\min_{\mathbf{u}} F = \sum_{k=1}^n (\alpha_u F_u[k] + \alpha_d F_d[k] + \alpha_\theta F_\theta[k] + \alpha_t F_t[k] + \alpha_o F_o[k]) \quad (7a)$$

$$s.t. \quad \mathbf{u}_{\min} \leq \mathbf{u}[k] \leq \mathbf{u}_{\max} \quad (7b)$$

$$\boldsymbol{\psi}_{\min} \leq \boldsymbol{\psi}[k] \leq \boldsymbol{\psi}_{\max} \quad (7c)$$

$$\mathbf{q}_{\min} \leq \mathbf{q}[k] \leq \mathbf{q}_{\max} \quad (7d)$$

$$d_{\min} \leq \|\boldsymbol{\chi}_1[k] - \boldsymbol{\chi}_2[k]\| \leq d_{\max} \quad (7e)$$

where  $\alpha_u, \alpha_d, \alpha_\theta, \alpha_t, \alpha_o$  are the weights of each term,  $\mathbf{u}_{\min} \in \mathbb{R}^4$ ,  $\mathbf{u}_{\max} \in \mathbb{R}^4$ ,  $\boldsymbol{\psi}_{\min} \in \mathbb{R}^4$ ,  $\boldsymbol{\psi}_{\max} \in \mathbb{R}^4$ ,  $\mathbf{q}_{\min} \in \mathbb{R}^{2m}$ ,  $\mathbf{q}_{\max} \in \mathbb{R}^{2m}$  are all constant vectors, that give the range of variables  $\mathbf{u}$ ,  $\boldsymbol{\psi}$ ,  $\mathbf{q}$ , respectively. While  $d_{\min}$  and  $d_{\max}$  are the positive constants, which gives the distance range between the two end robots. The objective function (7a) is comprised of several terms, each of which is explained as follows:

a) *Control input term.* To save the energy of the system, the control input term  $F_u$  is formulated as

$$F_u[k] = \mathbf{u}[k]^T Q_u \mathbf{u}[k] \quad (8)$$

where  $\mathbf{u}[k] = [v_1[k], \omega_1[k], v_2[k], \omega_2[k]]^T \in \mathbb{R}^4$  is the predicted control input (velocity and angle velocity) of two end mobile agents at  $k$ -th step,  $Q_u \in \mathbb{R}^{4 \times 4}$  is the positive definite matrix that can adjust the proportion of velocity  $v_i$  and angular velocity  $\omega_i$  of two end mobile robots.

b) *Distance error term.* This term can attract the flexible mobile agent system towards the target object. As mentioned in *Problem 1*, the envelope task requires  $\mathbf{p}_v$  converge to  $\mathbf{p}_t$ . So, this term is represented as:

$$F_d[k] = (\mathbf{p}^v[k] - \mathbf{p}_t)^T K_d (\mathbf{p}^v[k] - \mathbf{p}_t) \quad (9)$$

where  $K_d \in \mathbb{R}^{2 \times 2}$  is the positive definite matrix that can modify the ratio among various directions,  $\mathbf{p}^v[k]$  is the predicted virtual geometric central point at  $k$ -th step.

c) *Steer term.* To realize the control of the relative orientation, the steer term  $F_\theta[k]$  is formulated as  $-\cos\theta[k]$ . The calculation of the cosine factor is more straightforward, and it also represents the error between the orientation of the system and the direction needed to enclose the target object. The steer term can drive  $\theta$  to zero, indicating that the target object is completely situated on the ‘‘open’’ side of the system. Considering the symmetry of the tube, the  $\mathbf{r}_2$  is orthogonal to  $\boldsymbol{\chi}_1 - \boldsymbol{\chi}_2$  and the modulus of  $\mathbf{r}_2$  has no effect on this steer term. So,  $\mathbf{r}_2$  can be calculated as follows without involving the tube shape information, which can reduce the influence of the modeling error of the tube.

$$\mathbf{r}_2 = R_r(\boldsymbol{\chi}_1 - \boldsymbol{\chi}_2) = \begin{bmatrix} 0 & -1 \\ 1 & 0 \end{bmatrix} (\boldsymbol{\chi}_1 - \boldsymbol{\chi}_2) \quad (10)$$

where  $R_r$  is the rotation matrix for  $90^\circ$  counterclockwise rotation. One major challenge in optimizing a multi-task model is the conflicting gradients, which impact the performance of specific tasks [21]. To ensure the optimization of both targets (the distance error and the relative orientation), it is crucial to design the weights of  $F_d$  and  $F_\theta$ , considering their distinct units and ranges. Also, the two gradients both depend on

$\boldsymbol{\chi}_i$ , so it is necessary to update the weights of these two terms along the motion of this system. Thus, before each iteration of the optimization, the weight  $\alpha_\theta$  undergoes an update by the following rule to ensure that both targets have an equal influence on the direction of the objective function’s optimization.

$$\alpha_\theta = \frac{\alpha_d}{2} \sum_{i=1}^2 \left( \left\| \frac{\partial F_d}{\partial \boldsymbol{\chi}_i} \right\| / \left\| \frac{\partial F_\theta}{\partial \boldsymbol{\chi}_i} \right\| \right) \quad (11)$$

The gradient of  $F_\theta$  with respect to  $\boldsymbol{\chi}_i$  is calculated by:

$$\begin{aligned} \frac{\partial F_\theta}{\partial \boldsymbol{\chi}_i} &= -\mathbf{z}_2^T \frac{\partial \mathbf{z}_1}{\partial \boldsymbol{\chi}_i} - \mathbf{z}_1^T \frac{\partial \mathbf{z}_2}{\partial \boldsymbol{\chi}_i} = -\mathbf{z}_2^T \frac{\partial \mathbf{z}_1}{\partial \mathbf{r}_1} \frac{\partial \mathbf{r}_1}{\partial \boldsymbol{\chi}_i} - \mathbf{z}_1^T \frac{\partial \mathbf{z}_2}{\partial \mathbf{r}_2} \frac{\partial \mathbf{r}_2}{\partial \boldsymbol{\chi}_i} \\ &= \mathbf{z}_2^T \frac{(I_2 - \mathbf{z}_1 \mathbf{z}_1^T)}{\|\mathbf{r}_1\|} \mathbf{J}_i^M + (-1)^i \mathbf{z}_1^T \frac{(I_2 - \mathbf{z}_2 \mathbf{z}_2^T)}{\|\mathbf{r}_2\|} R_r \end{aligned} \quad (12)$$

where  $\mathbf{z}_1 = \mathbf{r}_1 / \|\mathbf{r}_1\|$ ,  $\mathbf{z}_2 = \mathbf{r}_2 / \|\mathbf{r}_2\|$ , and matrix  $\mathbf{J}_i^M \in \mathbb{R}^{2 \times 2}$  is the block of of  $\mathbf{J}(\boldsymbol{\psi})$  at the  $(2i-1)^{th}, (2i)^{th}$  columns and middle two rows. The gradient of  $F_d$  with respect to  $\boldsymbol{\chi}_i$  can be obtained by:

$$\begin{aligned} \frac{\partial F_d}{\partial \boldsymbol{\chi}_i} &= \frac{\partial F_d}{\partial \mathbf{p}^v} \frac{\partial \mathbf{p}^v}{\partial \boldsymbol{\chi}_i} = (\mathbf{p}^v - \mathbf{p}_t)^T (K_d^T + K_d) \frac{\partial \mathbf{p}^v}{\partial \boldsymbol{\chi}_i} \\ &= (\mathbf{p}^v - \mathbf{p}_t)^T (K_d^T + K_d) \frac{1}{m+2} \left( I_2 + \sum_{j=1}^m \mathbf{J}_i^j \right) \end{aligned} \quad (13)$$

where  $\mathbf{J}_i^j \in \mathbb{R}^{2 \times 2}$  is the block of  $\mathbf{J}(\boldsymbol{\psi})$  at the  $(2i-1)^{th}, (2i)^{th}$  columns and  $(2j-1)^{th}, (2j)^{th}$  rows. In order to prevent the steer term from restricting the flexibility of obstacle avoidance, the steer term  $F_\theta$  is activated only when the distance error falls below a specific threshold  $d_a$ , which means the system initiates a rotation towards the object, aligning itself to face the object with the open orientation.

d) *Target collision penalty term.* It is imperative to avoid any contact between the system and the object while executing the enveloping task. Similar to the repulsive potential field utilized in the artificial potential field approach [22], the collision penalty term is designed as:

$$F_t[k] = \sum_{i=1}^2 F_t^d(\boldsymbol{\chi}_i[k]) + \sum_{j=1}^m F_t^d(\mathbf{q}_j[k]) \quad (14)$$

where

$$F_t^d(\mathbf{q}) = \begin{cases} \frac{1}{2} k_t \left( \frac{1}{r_0} - \frac{1}{\|\mathbf{q} - \mathbf{p}_t\|} \right)^2 & \|\mathbf{q} - \mathbf{p}_t\| < r_0 \\ 0 & \text{else} \end{cases} \quad (15)$$

in which  $k_t > 0$  is the repulsive gain, and  $r_0$  is the allowed minimal distance between the mobile system and the target object. It is a soft constraint, which is equivalent to the inequality  $\|\mathbf{q} - \mathbf{p}_t\| \geq r_0$ . For feature points  $\mathbf{q}_j$ ,  $r_0$  can be set as the radius  $r_t$  of the minimum enclosing circle. For the end mobile robot  $\boldsymbol{\chi}_i$ , considering the radius of the robot,  $r_0 = r_t + r_e$ . Besides, the weight  $\alpha_t$  is designed to be large enough to ensure that this soft constraint will not be violated.

e) *Obstacle avoidance term.* The shape of the proposed system must be taken into consideration as our system cannot be perceived as a singular entity. The system is estimated to

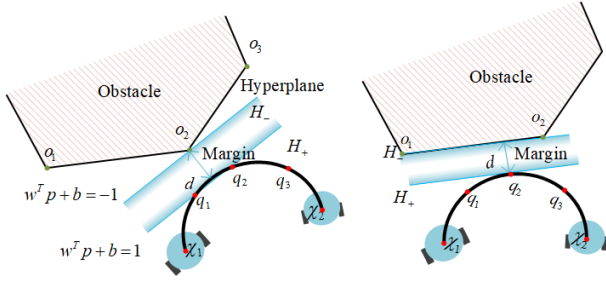


Fig. 4. The illustration of the margin between the flexible mobile agent system and the obstacle, that shows two types of different hyperplanes: (left) the hyperplane parallel to one side of the polygon  $\text{conv}$ ; (right) the hyperplane parallel to one side of the obstacle  $O$

be a convex polygon  $\text{conv} = \{\chi_1, \mathbf{q}_1, \dots, \mathbf{q}_m, \chi_2\}$ . And, the perceived obstacle information is donated by a point set  $O = \{\mathbf{o}_i \mid i = 1, 2, \dots\}$ , in which  $\mathbf{o}_i$  is the vertex or the point on the boundary of the obstacle sensed by robots. Hence, the max-margin method is introduced as a solution to avoid the obstacle, drawing inspiration from the supporting vector machine [23]. The following constrained quadratic programming problem obtains the hyperplanes with the max-margin between  $\text{conv}$  and  $O$ :

$$\begin{aligned} \min \quad & \frac{1}{2} \|\mathbf{w}\|^2, \\ \text{s.t.} \quad & z_i (\mathbf{w}^T \mathbf{p}_i + b) \geq 1, \quad \forall \mathbf{p}_i \in \text{conv} \cup O \end{aligned} \quad (16)$$

where  $z_i = 1$  if  $\mathbf{p}_i \in \text{conv}$ , otherwise,  $z_i = -1$ . And  $\mathbf{w} \in \mathbb{R}^2$  and  $b \in \mathbb{R}$  are the parameters of the hyperplanes  $H_-$  and  $H_+$ , as shown in Fig. 4. The inequality constraint ensures that the obstacle and the agent system are positioned on the opposite side of  $H_-$  and  $H_+$ , respectively. The margin  $d$ , also known as the distance between  $H_-$  and  $H_+$ , can be calculated by  $d = \frac{2}{\|\mathbf{w}\|}$ . To maximize  $d$ , the optimization target is to minimize  $\|\mathbf{w}\|$ . Then, by the Lagrangian multiplier method, we can get

$$L_{(\mathbf{w}, b, \lambda)} = \frac{1}{2} \|\mathbf{w}\|^2 + \sum_{\mathbf{p}_i \in \text{conv} \cup O} \lambda_i (1 - z_i (\mathbf{w}^T \mathbf{p}_i + b)) \quad (17)$$

According to the KKT (Karush-Kuhn-Tucker) condition, the Hyperplane  $H_-$  can be represented as

$$\sum_{\mathbf{p}_i \in \text{conv} \cup O} \lambda_i z_i \mathbf{p}_i^T \mathbf{p} + 1 = 0 \quad (18)$$

By solving the quadratic programming problem (16), the hyperplane  $H_-$  can be obtained in real time. Then, the obstacle avoidance term is designed as follows:

$$F_o[k] = \sum_{\mathbf{h}_i \in \text{conv}} F_h(\mathbf{h}_i) \quad (19)$$

$$\text{where } F_h(\mathbf{h}_i) = \begin{cases} 1 + \cos\left(\pi \frac{d(\mathbf{h}_i)}{d_{\min}}\right), & d(\mathbf{h}_i) < d_{\min} \\ 0, & \text{else} \end{cases} \quad (20)$$

and with  $d_{\min} > 0$  as the minimum safe margin. And  $d(\mathbf{h}_i)$  represents the distance between  $\mathbf{h}_i$  and the hyperplane  $H_-$ , which is calculated by

$$d(\mathbf{h}_i) = (\mathbf{w}^T \mathbf{h}_i + b + 1) / \|\mathbf{w}\| \quad (21)$$

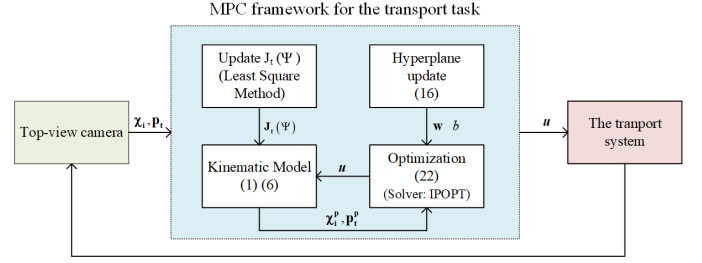


Fig. 5. Schematic overview of the framework for the transport task

The bump function  $F_h(h_i)$  is a repulsive potential function in the artificial potential field used in [24]. This function specifically ensures that the repulsive potential is active only when the distance  $d(\mathbf{h}_i)$  is smaller than the safety margin  $d_{\min}$ . Also, to ensure this soft constraint is not violated, the weight  $\alpha_o$  needs to be large enough.

*Constraints:* The constraints (7b) are the limitations of velocity and angular velocity.  $v_i$  may have a positive or negative value, indicating forward or backward movement respectively.  $\omega_i$  also can be negative or positive, indicating a turn to the left or right, respectively. The constraints (7c) and (7d) make sure the flexible mobile agent system moves in the rectangular bounded environment. Inequality (7e) expresses the distance limits between two agents, which should be neither too close, causing the collision, nor too far to extend the tube. So, this range is related to both the length of the tube and the radius of the mobile robots.

## B. Transport Problem Formulation

After finishing enveloping the object, the next stage is to transport the object to the target receptacle. During this process, the controlled plant is the whole transport system instead of the mobile agent. The new algorithm framework is shown in Fig. 5. The corresponding optimization problem of this process is constrained by (i) dynamics (1) and (6), (ii)–(iv) and (vi) from the enveloping problem, and (vii) the new pulling constraint. The optimal tasks are the distance error and the control input. This optimization problem is built as

$$\min_{\mathbf{u}} \tilde{F} = \sum_{k=1}^n \left( \tilde{\alpha}_u \tilde{F}_u[k] + \tilde{\alpha}_d \tilde{F}_d[k] + \tilde{\alpha}_o \tilde{F}_o[k] \right) \quad (22a)$$

$$\text{s.t.} \quad \mathbf{u}_{\min} \leq \mathbf{u}[k] \leq \mathbf{u}_{\max} \quad (22b)$$

$$\boldsymbol{\psi}_{\min} \leq \boldsymbol{\psi}[k] \leq \boldsymbol{\psi}_{\max} \quad (22c)$$

$$d_{\min} \leq \|\chi_1 - \chi_2\| \leq d_{\max} \quad (22d)$$

$$\tilde{\mathbf{p}}_{\min} \leq \tilde{\mathbf{p}}_t[k] \leq \tilde{\mathbf{p}}_{\max} \quad (22e)$$

$$y_t^b[k+1] \geq 0 \quad (22f)$$

where  $\tilde{\alpha}_u$ ,  $\tilde{\alpha}_d$ ,  $\tilde{\alpha}_o$  are the constant weights of each term. Different from the enveloping process, this objective function contains three parts. The control input term  $\tilde{F}_u$  is the same as (8). The distance error between the transported object  $\tilde{\mathbf{p}}_t$  and the target zone  $T_z$  is represented by:

$$\tilde{F}_d[k] = (\mathbf{p}_t[k] - T_z)^T \tilde{K}_d (\mathbf{p}_t[k] - T_z) \quad (23)$$

where  $\tilde{K}_d \in \mathbb{R}^{2 \times 2}$  is the positive definite matrix.

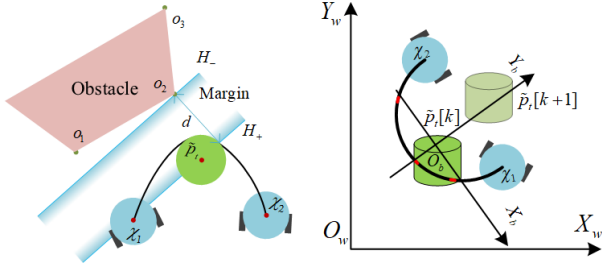


Fig. 6. (left) The illustration of the margin between the whole transport system and the obstacle. (right) The body frame of the transport system

As shown in the left subfigure of Fig. 6, considering the object may occlude the tube in the view of the camera, the detection of feature points of the tube might be challenging. Also, due to the pulling force applied, the deformable tube between the object and the end robot will stretch and morph into a nearly straight shape. Then, the entire system is considered as a flexible triangle with the two end-robots and the object being transported forming the three vertices of it. So, for the obstacle avoidance term, the feature points  $\mathbf{q}_i$  are replaced by the center point  $\tilde{\mathbf{p}}_t$  of the transposed object, the new convex polygon of this system is  $\text{conv}_t = \{\chi_1, \tilde{\mathbf{p}}_t, \chi_2\}$  and the corresponding obstacle avoidance term is:

$$\tilde{F}_o[k] = \sum_{\mathbf{h}_i \in \text{conv}_t} F_h(\mathbf{h}_i) \quad (24)$$

Taking into account the distance between the center point of the transported object and its boundary, the safety margin  $d_{\min}$  needs to be bigger compared to the enveloping process.

*Constraints:* The constraints (22b)–(22d) are the same as the enveloping problem. The constraint (22e) is to make sure that the transported object also moves in the rectangular bounded environment. The inequality (22f) expresses the motion constraint of the pulling manipulation. The body frame  $\sigma_b$  is shown as in the right subfigure of Fig. 6, where the origin  $O_b$  is defined as the center of the transported object  $\tilde{\mathbf{p}}_t$ . The direction of the  $X_b$  axis is determined by the two end mobile robots, which is parallel to the vector  $\chi_1 - \chi_2$ . The predicted next step position  $\mathbf{p}_t^b[k+1]$  of the transported object under the body frame  $\sigma_b[k]$  is calculated by

$$\mathbf{p}_t^b[k+1] = \begin{bmatrix} \cos\phi[k] & \sin\phi[k] \\ -\sin\phi[k] & \cos\phi[k] \end{bmatrix} (\mathbf{p}_t[k+1] - \mathbf{p}_t[k]) \quad (25)$$

where  $\mathbf{p}_t^b[k+1] = [x_t^b[k+1], y_t^b[k+1]]^T \in \mathbb{R}^2$ ,  $\phi[k]$  is the angle of the vector  $\chi_1 - \chi_2$  in the world frame at the  $k$ -th step and calculated by

$$\phi[k] = \text{atan2}(y_1[k] - y_2[k], x_1[k] - x_2[k]) \quad (26)$$

The non-negative constraint of  $\tilde{\mathbf{p}}_t[k+1]$  on  $Y_b[k]$  direction implies that the transported object will not move backward, which ensures the pulling constraint. Through the inequality (22f), the system can realize the forward pulling and the rotating in place with the transported object as the center, which shows the flexibility of our system.

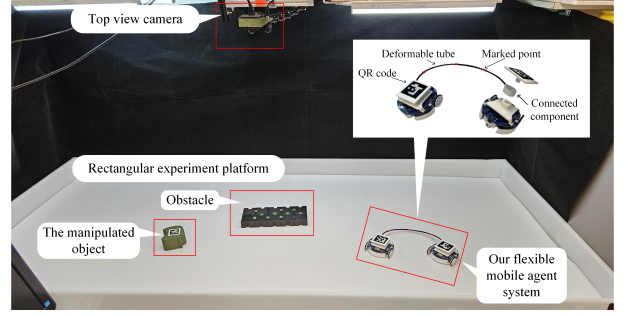


Fig. 7. Details of the experimental platform used to validate the method.

## IV. RESULTS

### A. Setup

As shown in Fig. 7, we conducted this experimental study on a bounded rectangular platform with a size of 140 cm  $\times$  80 cm. The flexible mobile agent system consists of two Mona robots [25] and one 30 cm-long deformable tube. By the connected component, the end of the tube is attached to the end robot but can rotate flexibly, making the shape of the tube relatively fixed and suitable for transport. The top-view camera obtains the state feedback information of the flexible mobile agent system and the manipulated object. To get the shape information of the tube, we add some red markers evenly on the tube as the feature points and use the OpenCV libraries to process the images and track the feature points. The number of feature points considered the size of the target object to ensure that the object could not pass between two adjacent feature points. So, in our experiment, we used three feature points, that is,  $m = 3$ . The receptacle zone is designed as a rectangle zone at one corner of the platform. The Mona robots' linear velocity and angular velocity are regulated wirelessly by a host PC. In our experiments, the time step of MPC is set as 0.15 s. The prediction horizon  $N$  is 30, and the control step  $N_s$  is 4. The max velocity of the robots is designed as 0.15 m/s, and the max angle velocity is 0.4 rad/s. The activated distance  $d_a$  of the steer term is set as 0.35 m. The distance constraints of two mobile robots are set as  $d_{\min} = 12$  cm and  $d_{\max} = 27$  cm to avoid the collision of two agents and the extend of the tube.

We solve the proposed nonlinear constrained optimization problems (7) and (22) by Interior Point OPTimizer (IPOPT) solver [26], which is a software library for large-scale nonlinear optimization of continuous systems. Due to the control step  $N_s = 4$ , the predicted control inputs of 5-th step and beyond can be set as the initial guesses of the next optimization. The initial values of control inputs without the predicted value are set to zero. Videos of the experiments can be found at <https://vimeo.com/917007028>.

### B. Real-World Experiments

1) *Experiments without Obstacles:* First, the proposed algorithm is evaluated by conducting tests using objects of various shapes placed at different locations in an environment without any obstacles. Fig. 8 illustrates the process of envelopment and transportation of three different cases. The light snapshots are the states during this process, while the dark snapshots are

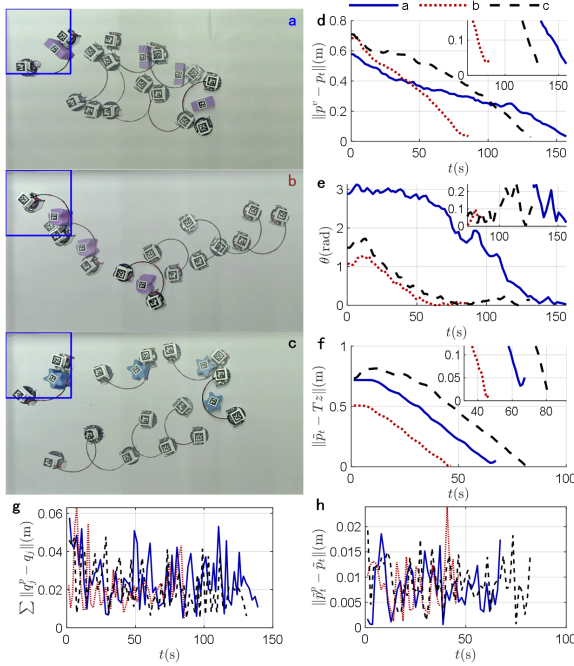


Fig. 8. Snapshots of three experiments of different objects by our flexible mobile agent system in the no obstacle situation a–c and the corresponding quantitative results d–h

each task’s final configuration. The blue rectangle of the top left corner is the target receptacle. Objects with diverse shapes, including both convex and nonconvex shapes, are tested to demonstrate the adaptability of our proposed system.

The quantitative experiment results are also given in Fig. 8 d–h. The superscript “ $p$ ” presents the corresponding predicted variable. When the direction error  $\|\mathbf{p}^v - \mathbf{p}_t\|$  and the relative orientation  $\theta$  are both close enough to zero, the enveloping task is finished. In the experiment *a*, it is clear that the steering term is activated at around 70 s, and the system starts rotating to face the object with the “open” side. As shown in Fig. 8 g, the error  $\sum_j^m \|q_j^p - q_j\|$ , that represents the error in predicting the position of the tube, is most fall in the 6 cm bound, which is acceptable for our task. The position prediction errors of the transported object are also depicted in Fig. 8 h, exhibiting values close to zero and falling within the range of  $\pm 3$  cm.

*Remark.* The model errors of the tube and transported objects can not converge to zero strictly in experiments. The models are not fixed and are affected by the relative configuration of the system, which is not strictly quasi-static throughout the motion process. However, the error of the proposed estimated model is acceptable in our task.

2) *Experiments with Obstacles:* To test the performance of obstacle avoidance, a series of manipulation tasks with obstacles of different shapes are conducted. Fig. 9 presents four sets of experimental results. A snake-shaped obstacle (Fig. 9. a) and a rectangular obstacle (Fig. 9. b–d) are used to represent the non-convex and convex obstacles, respectively. To avoid overlapping snapshots, the enveloping and transport processes of **d** have been divided into **d. 1** and **d. 2**. The performed experiments involve obstacle avoidance on the lateral sides of the two end robots (Fig. 9. a, d) and on the side

of the tube (Fig. 9. b, c) during the enveloping task. Fig. 9. c, d also shows the avoidance of obstacles during the transportation process. As shown in Fig. 9. e–f, two optimization targets of the enveloping problem, the distance error  $\|\mathbf{p}^v - \mathbf{p}_t\|$  and the relative orientation  $\theta$ , have both converged to zero. Also, the transported objects are positioned within the designated area with permissible deviations. In conclusion, our system has completed the task of envelopment and transport with obstacles of varying shapes and target objects positioned differently.

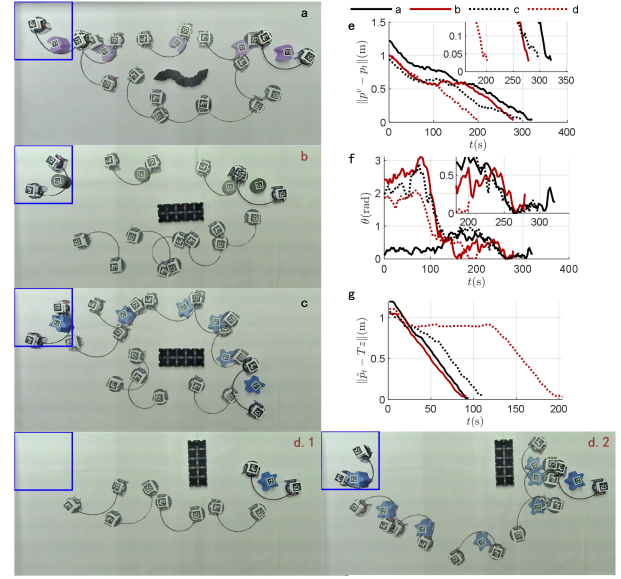


Fig. 9. Snapshots of experiments of the proposed method applied in different obstacle situations a–d and the corresponding quantitative results e–g.

*Remark.* The chattering of the two mobile robots is mainly due to measurement errors, such as position or orientation, and inaccurate predictive models. Using mobile robots with stepping motors such as e-puck2 and an optical motion capture system of location may help to improve performance.

*Remark.* Our framework has the potential to be applied to multiple object manipulations. This is possible if the object clusters can be enclosed within a disk that adheres to the size constraint (4) for the enveloping task and if the geometric center of these object clusters can be continuously detected in real-time throughout the transportation process. A brief related experiment can also be found in the above video link.

3) *Comparison:* For obstacle avoidance during the enveloping process, the comparison of our maximum margin method and the classic Artificial Potential Field (APF) is conducted, and the results are given in Table I and Table II of Fig. 10. In APF, the repulsive potential fields in [27] of each feature point  $\mathbf{q}_j$  and the two agent robots  $\chi_i$  are considered and added to the objective function (7a). The comparison experiments are conducted using rectangular obstacles of varying sizes, made up of different numbers of cubes. The two methods use the same state feedback and the same safe margin. Failure cases of APF in Fig. 10 show that the two ends of the tube tend to extend in different directions when sensing the obstacles. It is primarily due to the conflicting repulsive potential fields

Size of Obstacle	Ours	APF
2×4	Yes (3/3)	No (0/3)
1×4	Yes (3/3)	No (0/3)
1×2	Yes (3/3)	No (0/3)

The ratios represent the successful runs (i.e., bypassed obstacles), for a total of three runs.

Method	$t_{avg}$ (s)	$t_{min}$ (s)	$t_{max}$ (s)
Ours	1.128	0.511	1.484
APF	1.143	0.764	1.672

Failure cases of APF

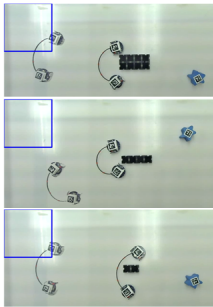


Fig. 10. Comparison of our proposed obstacle avoidance method and APF under different size obstacles. In the failure cases, the light snapshots are the initial position of our system.

that exist within different components of the system with a linear shape. In contrast, our proposed approach exactly avoids this potential hazard. Moreover, the computation time required to solve the optimization problem (7) once, resulting in the determination of the subsequent control inputs for the next four steps, is presented in TABLE II. Ours has shorter computation times, which is more significant when dealing with a system with more feature points.

*Remark.* Infeasibility problems may occur in optimization-based frameworks. The constraints in our frameworks are mainly physical limitations that can not be relaxed. Considering that the weights of the terms in the objective function reflect the relative priorities of the multiple objectives, temporarily removing them with lower weight may help identify a feasible solution for an infeasible optimization problem.

## V. CONCLUSION

In this paper, the problem of nonprehensile object manipulation by the proposed flexible mobile agent system has been addressed. The proposed system consists of two mobile end robots linked by a deformable tube, which shows the potential for object manipulation by the deformable material. The corresponding local planning and control frameworks of the proposed new system for object enveloping and transport are presented and successfully tested with real experiments. The position and orientation requirements and obstacle avoidance, nonprehensile manipulation are all formulated and integrated into the optimization problem.

Our work shows the possibilities and challenges associated with nonprehensile manipulation using the combination of deformable materials and mobile robots. In future work, to utilize this system's flexibility, the path planning algorithm considered nonholonomic properties will be further developed, which can effectively handle complex or crowded scenarios and manipulate multiple objects.

## REFERENCES

- [1] W. Ma, B. Zhang, L. Han, S. Huo, H. Wang, and D. Navarro-Alarcon, "Action planning for packing long linear elastic objects into compact boxes with bimanual robotic manipulation," *IEEE/ASME Trans. Mechatron.*, vol. 28, no. 3, pp. 1718–1729, 2023.
- [2] H. Chen, W. Wan, and K. Harada, "Combined task and motion planning for a dual-arm robot to use a suction cup tool," in *IEEE Int. Conf. Humanoid Robot.*, 2019, pp. 446–452.

- [3] H. Ebel and P. Eberhard, "Non-prehensile cooperative object transportation with omnidirectional mobile robots: Organization, control, simulation, and experimentation," in *2021 International Symposium on Multi-Robot and Multi-Agent Systems (MRS)*. IEEE, 2021, pp. 1–10.
- [4] "Projects.the ocean cleanup," <https://theoceancleanup.com/projects/>.
- [5] N. Melenbrink, J. Werfel, and A. Menges, "On-site autonomous construction robots: Towards unsupervised building," *Autom. Constr.*, vol. 119, p. 103312, 2020.
- [6] J. Kim, A. K. Mishra, R. Limosani, M. Scafuro, N. Cauli, J. Santos-Victor, B. Mazzolai, and F. Cavallo, "Control strategies for cleaning robots in domestic applications: A comprehensive review," *Int. J. Adv. Robot. Syst.*, vol. 16, no. 4, p. 1729881419857432, 2019.
- [7] E. Tuci, M. H. Alkilabi, and O. Akanyeti, "Cooperative object transport in multi-robot systems: A review of the state-of-the-art," *Front. Rob. AI*, vol. 5, p. 59, 2018.
- [8] K. Hunte and J. Yi, "Collaborative object manipulation through indirect control of a deformable sheet by a mobile robotic team," in *IEEE 15th International Conference on Automation Science and Engineering*, 2019, pp. 1463–1468.
- [9] J. Alonso-Mora, S. Baker, and D. Rus, "Multi-robot navigation in formation via sequential convex programming," in *2015 IEEE/RSJ Int. Conf. Intell. Robots Syst.* IEEE, 2015, pp. 4634–4641.
- [10] J. Alonso-Mora, R. Knepper, R. Siegwart, and D. Rus, "Local motion planning for collaborative multi-robot manipulation of deformable objects," in *IEEE Int. Conf. Robot. Autom.* IEEE, 2015, pp. 5495–5502.
- [11] G. Sun, R. Zhou, Z. Ma, Y. Li, R. Groß, Z. Chen, and S. Zhao, "Mean-shift exploration in shape assembly of robot swarms," *Nat. Commun.*, vol. 14, no. 1, p. 3476, 2023.
- [12] F. R. Hogan and A. Rodriguez, "Reactive planar non-prehensile manipulation with hybrid model predictive control," *Int. J. Rob. Res.*, vol. 39, no. 7, pp. 755–773, 2020.
- [13] F. Bertonecchi, F. Ruggiero, and L. Sabattini, "Linear time-varying mpc for nonprehensile object manipulation with a nonholonomic mobile robot," in *IEEE Int. Conf. Robot. Autom.*, 2020, pp. 11 032–11 038.
- [14] F. Bertonecchi, M. Selvaggio, F. Ruggiero, and L. Sabattini, "Task-oriented contact optimization for pushing manipulation with mobile robots," in *IEEE Int. Conf. Intell. Robots Syst.*, 2022, pp. 1639–1646.
- [15] S. Rodriguez, M. Morales, and N. M. Amato, "Multi-agent push behaviors for large sets of passive objects," in *2016 IEEE/RSJ Int. Conf. Intell. Robots Syst.*, 2016, pp. 4437–4442.
- [16] S. Kuroki, T. Matsushima, J. Arima, H. Furuta, Y. Matsuo, S. Gu, and Y. Tang, "Collective intelligence for 2d push manipulations with mobile robots," *IEEE Robot. Autom. Lett.*, vol. 8, no. 5, pp. 2820–2827, 2023.
- [17] Y. Su, Y. Jiang, Y. Zhu, and H. Liu, "Object gathering with a tethered robot duo," *IEEE Robotics and Automation Letters*, vol. 7, no. 2, pp. 2132–2139, 2022.
- [18] Y. Huang and S. Zhang, "Cooperative object transport by two robots connected with a ball-string-ball structure," *IEEE Robotics and Automation Letters*, 2024.
- [19] Z. Feng, G. Hu, Y. Sun, and J. Soon, "An overview of collaborative robotic manipulation in multi-robot systems," *Annu. Rev. Control.*, vol. 49, pp. 113–127, 2020.
- [20] D. Navarro-Alarcon and Y.-H. Liu, "Fourier-based shape servoing: A new feedback method to actively deform soft objects into desired 2-d image contours," *IEEE Trans. Rob.*, vol. 34, no. 1, pp. 272–279, 2018.
- [21] B. Liu, X. Liu, X. Jin, P. Stone, and Q. Liu, "Conflict-averse gradient descent for multi-task learning," *Advances in Neural Information Processing Systems*, vol. 34, pp. 18 878–18 890, 2021.
- [22] A. Nasuha, A. Priambodo, and G. Pratama, "Vortex artificial potential field for mobile robot path planning," in *J. Phys. Conf. Ser.*, vol. 2406, no. 1. IOP Publishing, 2022, p. 012001.
- [23] M. A. Hearst, S. T. Dumais, E. Osuna, J. Platt, and B. Scholkopf, "Support vector machines," *IEEE Intell. Syst. Appl.*, vol. 13, pp. 18–28, 1998.
- [24] S. Park and S. Lee, "Formation reconfiguration control with collision avoidance of nonholonomic robots," *IEEE Robot Autom Lett*, 2023.
- [25] F. Arvin, J. Espinosa, B. Bird, A. West, S. Watson, and B. Lennox, "Mona: an affordable open-source mobile robot for education and research," *J. Intell. Robot. Syst.*, vol. 94, pp. 761–775, 2019.
- [26] A. Wächter and L. T. Biegler, "On the implementation of an interior-point filter line-search algorithm for large-scale nonlinear programming," *Math. Program.*, vol. 106, pp. 25–57, 2006.
- [27] P. Wang, S. Gao, L. Li, B. Sun, and S. Cheng, "Obstacle avoidance path planning design for autonomous driving vehicles based on an improved artificial potential field algorithm," *Energies*, vol. 12, p. 2342, 2019.